EVOLUTIONARY BIOLOGY

Cross-species implementation of an innate courtship behavior by manipulation of the sex-determinant gene

Ryoya Tanaka[1,2*†], Yusuke Hara[2†], Kosei Sato[2], Soh Kohatsu[2], Hinata Murakami[3], Tomohiro Higuchi[3], Takeshi Awasaki[4], Shu Kondo[5], Atsushi Toyoda[6], Azusa Kamikouchi[1,3], Daisuke Yamamoto[2*]

In accepting a courting male, *Drosophila subobscura* females require nuptial gift giving in which a male gives regurgitated crop contents to her mouth to mouth. No similar behavior is found in *D. melanogaster*. By clonal activation of neurons expressing the male-determinant FruM, we identified insulin-like peptide–producing cells (IPCs) and their putative postsynaptic targets, proboscis-innervating motoneurons, as those critical for gift giving. We demonstrate that loss of FruM from *D. subobscura* IPCs abrogates neurite extension and gift giving, whereas FruM overexpression in their *D. melanogaster* counterparts induces overgrowth of neurites that harbor functional synapses, culminating in increased regurgitation. We suggest that the acquisition of FruM expression by IPCs was a key event occurring in an ancestral *D. subobscura* that conferred a latent capability to perform nuptial gift giving.

What is the neural mechanism that determines the presence or absence of a specific action in an otherwise conserved innate behavior? As a first step in addressing this question, we focused on nuptial gift giving (NGG) in the courtship ritual of *Drosophila subobscura*, a species separated from the *D. melanogaster* lineage ~30 to 35 million years ago (*1*–*3*). The male fly presents a droplet of regurgitated crop contents on his mouth tip in front of a female fly, who may extend her proboscis and suck up the droplet (Fig. 1, A and B). No *Drosophila* species other than *D. subobscura* exhibits any similar behavior (Fig. 1, C to I, and movies S1 and S2) (*4*), with the single exception of *D. persimilis*, the males of which occasionally show similar NGG, although this behavior is dispensable for female acceptance (*5*). By thermogenetically stimulating a few neurons that express sex-specific products of the *fruitless* (*fru*) gene FruM (*6*, *7*) by means of stochastic mosaicism, we have identified a few subsets of *fru* neurons that are capable of eliciting courtship-associated regurgitation in *D. subobscura*.

Clonal stimulation of *fru* neurons induces regurgitation

To conduct mosaic analysis of NGG, we genome edited *D. subobscura* so that the flies carried three constructs, *fru*^{so}*-GAL4*, *UAS>STOP>dTrpA1::Myc*, and *hs-flp*, a minimal triad required for generating simple flip-out clones of a small number of *fru* neurons (fig. S1, A and B). Because *dTrpA1* encodes a cation channel that opens at temperatures around 30°C, the ambient temperature was increased from 18° to 29°C to determine whether the test flies exhibited regurgitation in response to this temperature change. We obtained two fly groups: a regurgitation-positive and a regurgitation-negative group. Their brains were then dissected and subjected to anti-Myc antibody staining to visualize neurons expressing *dTrpA1::Myc*, which had been thermogenetically activated in behavioral assays. The neurons thus visualized were scarce, although heterogeneous neuron populations were present, allowing us to identify

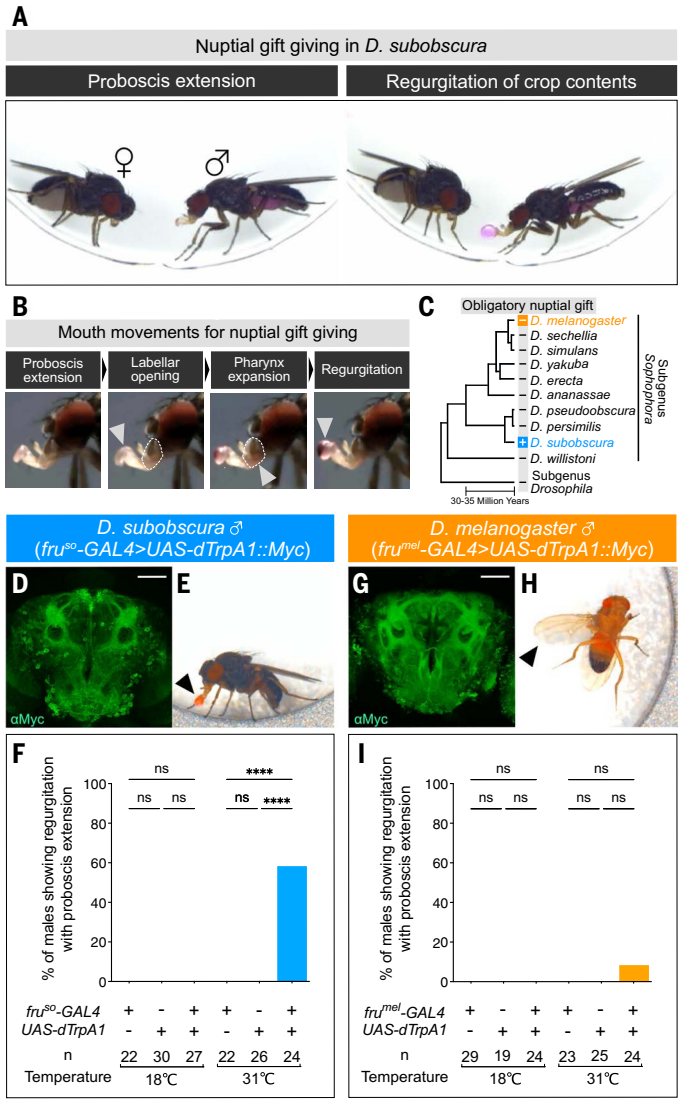

Fig. 1. NGG in *D. subobscura*. (**A**) Male proboscis extension (left) and regurgitation (right) in preparation for the gift of a droplet. (**B**) Mouth movements for NGG: proboscis extension, labellar opening (arrowhead: widened labellum), pharynx expansion (arrowhead: enlarged pharynx; compare the contours of the constricted and dilated pharynx shown with broken lines in the middle left and middle right panels) and regurgitation (the arrowhead: a droplet). (**C**) Phylogenetic tree (branches not to scale) highlighting the presence (+) or absence (−) of reported evidence for obligatory NGG. (**D** to **I**) The *fru* circuit [(D) and (G)] that induces courtship actions [(E), (F), (H), and (I)] in *D. subobscura* [(D) to (F)] and *D. melanogaster* [(G) to (I)] males. (D and G) Anterior view of the *fru* circuit visualized with *fru-GAL4*. Scale bar, 50 μm. (E and H) Courtship actions (arrowheads) induced by *dTrpA1* activation (regurgitation in *D. subobscura*; wing extension in *D. melanogaster*). (F and I) Quantification of regurgitation induced by activation of the *fru* circuit in *D. subobscura* (F) and *D. melanogaster* (I) males. ****$P <$ 0.0001; ns, not significant by the Fisher's exact test for count data and the Hochberg method for *P* value adjustment (table S6).

[1]Division of Biological Science, Graduate School of Science, Nagoya University, Nagoya, Aichi, Japan. [2]Advanced ICT Research Institute, National Institute of Information and Communications Technology, Kobe, Hyogo, Japan. [3]Graduate School of Life Sciences, Tohoku University, Sendai, Miyagi, Japan. [4]Department of Biology, School of Medicine, Kyorin University, Mitaka, Tokyo, Japan. [5]Department of Biological Science and Technology, Faculty of Advanced Engineering, Tokyo University of Science, Katsushika, Tokyo, Japan. [6]Advanced Genomics Center, National Institute of Genetics, Mishima, Shizuoka, Japan. ***Corresponding author. Email: tanaka.ryoya.z3@f.mail.nagoya-u.ac.jp (R.T.); daichan@nict.go.jp (D.Y.)**
†These authors contributed equally to this work.

major groups of *fru* neurons (Fig. 2, A and B, and tables S1 and S2) in *D. subobscura* males based on anatomical similarities to putative homologous neurons in *D. melanogaster* (*8*–*10*). For the *fru* neurons in the subesophageal ganglion (SG), we tentatively divided them into four large heterogeneous groups: lateral (L), medial (M), anterior (a), and posterior (p) neurons (Fig. 2B). We then calculated the proportion of mosaic flies in which each neural group was activated during the thermogenetic behavioral assays (the active-upon-warming score or A-score; Fig. 2C and tables S1 and S2). We reasoned that the neural groups in which the A-score was higher for the regurgitating than the nonregurgitating fly group would be promising candidates for neurons contributing to regurgitation. We should note, however, that regurgitation is known to occur after the ingestion of a large amount of liquid food in various flies (fig. S2, A and B) (*11*, *12*), and this assay alone does not distinguish NGG-associated regurgitation from postfeeding regurgitation.

Insulin neurons promote NGG

Two neuronal groups attracted our attention, pars intercerebralis (PI) neurons and L-pSG neurons, because they were labeled more often in the regurgitating than in the nonregurgitating fly group (Fig. 2C and tables S1 and S2). Note, however, that a substantial proportion (38.5%) of nonregurgitating flies carried anti-Myc–labeled PI neurons. This is presumably because dTrpA1 was also expressed in other neurons that suppress regurgitation (tables S1 and S2). The PI neurons labeled in regurgitating mosaic flies resembled insulin-like peptide–producing cells (IPCs) in *D. melanogaster* (Fig. 2A) (*13*). To test whether IPCs are involved in NGG, these neurons were thermogenetically activated through the *dilp2*^{sopA}*-GAL4* driver (Fig. 3, A and B, and fig. S3, A to H). We found that IPC activation substantially increased the incidence of NGG (Fig. 3C), and the probability of observing regurgitation in response to elevated temperature increased as the number of *dTrpA1*-expressing IPCs increased (fig. S1C). Conversely, the males carrying inactivated IPCs engaged less frequently in NGG than did control males (Fig. 3D). Furthermore, the *dilp2* mutant males showed a reduction in the number of NGGs compared with control males (Fig. 3E). However, general courtship activities as measured by the courtship index were not affected by IPC activation, IPC inactivation, or the *dilp2* mutation (fig. S4, A to C). Additionally, in solitary males, thermogenetic activation of IPCs similarly promoted regurgitation (fig. S4D). These observations indicate that IPCs accelerate NGG.

We then investigated whether activities in IPCs affect male fitness. Single females were given a choice between two males, one carrying IPCs activated through dTrpA1 and the other carrying IPCs with no dTrpA1, to determine which males were more successful in mating. Our results showed that IPC-activated males copulated at a higher rate than unmanipulated males under such competitive conditions (Fig. 3F). We conclude that IPCs are positive modulators of NGG, and IPC activities may confer higher fitness on males.

Insulin neurons are recruited to the courtship circuit

To clarify whether IPCs express FruM in these two *Drosophila* species, IPCs were doubly stained with anti-FruM and anti-Dilp2 antibodies (Fig. 3G and fig. S5, A and B). Sixteen to 18 IPCs were marked with the anti-sDilp2, and most (16 or 17) of these were also labeled with anti-FruM in *D. subobscura* (Fig. 3G, left, and table S3). By contrast, none of 16 *D. melanogaster* IPCs were labeled by anti-FruM (Fig. 3G, right, and table S3), suggesting that IPCs express FruM in *D. subobscura* but not in *D. melanogaster*.

Courtship initiator P1 neurons modulate IPC activities

In *D. melanogaster*, male-specific P1 neurons (20/hemisphere) in the *fru* circuit play a role in triggering courtship (*9*). We found that compared with those of their *D. melanogaster* counterparts, apical dendrites of *D. subobscura* IPCs were substantially longer and extended laterally (Fig. 3, H and J). To generate a P1-specific GAL4, we introduced a *D. melanogaster*–derived enhancer sequence (*R71G01-GAL4*) or its homologous *D. subobscura* sequence into the *D. subobscura* genome. However, neither transgene yielded GAL4 expression in P1 neurons in *D. subobscura*. As an alternative approach, *Venus* inserted into the *fru* second exon, which was fused with *Chrimson* (*fru*$^{Chirimson::Venus}$), was used to label the entire *fru* circuit (*3*). This visualized a neurite extruding from the lateral junction of the *fru* circuit, which appeared to contact the dendrites of *D. subobscura* IPCs (fig. S6). We next examined the effect of *fru* knockdown targeted to IPCs (fig. S7A) on neurite structures and on NGG performance in *D. subobscura* males. *fru* knockdown led to not only a loss of elongated dorsolateral arbors but also to a reduction in the incidence of NGG (Fig. 3, I, K, and L). By contrast, *fru* knockdown had no effect on the number of IPCs (fig. S7B). Next, we optogenetically stimulated the entire *fru* circuit while recording membrane electrical responses from an IPC. LED illumination induced excitatory responses in the IPC, which were diminished by Ca^{2+} deprivation that blocks synaptic activities, leaving the nonsynaptic component intact. Subtracting the nonsynaptic component from the total response recorded from

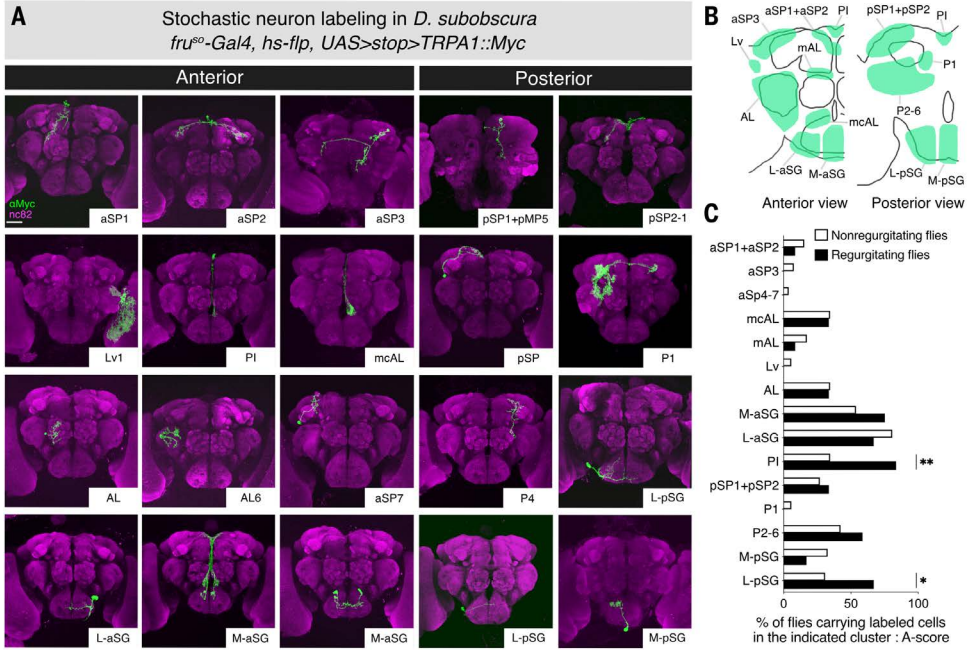

Fig. 2. Flip-out mosaicism identifies *fru*-positive neuronal groups that induce regurgitation upon activation in *D. subobscura* males. (**A**) Examples of clones of different neuronal groups obtained by partial stacks of original images. The names of the neuronal groups are indicated below each image. Scale bar, 50 μm. (**B**) Schematic drawing of the locations of neuronal clusters defined in this study. Anterior (left) and posterior (right) views are shown. (**C**) Behavioral assay results with mosaic flies. Proportions (abscissa: A-score, %) of flies carrying *dTrpA1*-expressing clones in the indicated neural cluster for regurgitating (solid bars) and nonregurgitating (open bars) groups are shown. Fisher's exact test was used for statistical analysis of count data (table S6). $^{**}P < 0.01$; $^{*}P < 0.05$.

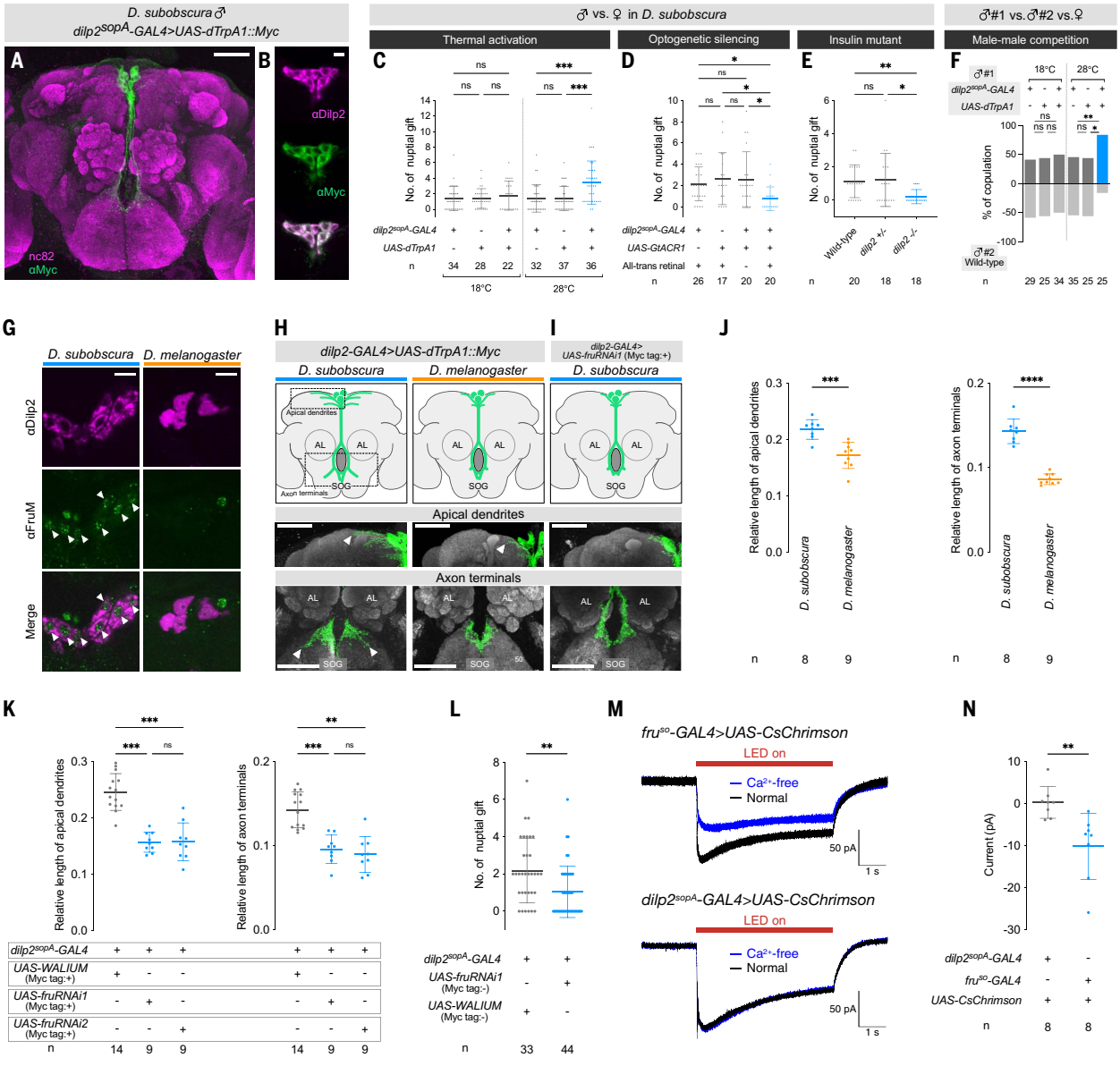

Fig. 3. Importance of FruM expression for NGG. (**A**) IPCs of *D. subobscura* males. (**B**) Double staining with anti-sDilp2 (top) and anti-Myc (middle) and the merged images (bottom). (**C** to **E**) Effects of IPC activation (C), inactivation (D), or *dilp2* mutants (E) on NGG. (**F**) Effect of IPC activation on competitive mating. (**G**) Double staining with anti-Dilp2 (top) and anti-FruM (middle) in *D. subobscura* (left) and *D. melanogaster* (right) and the merged images (bottom). Arrowheads: anti-FruM–positive nuclei. (**H** and **I**) Examples (bottom) and schematics (top) of IPC neurites in *D. subobscura* [(H), left], *D. melanogaster* [(H), right] and *D. subobscura* with *fru* knockdown (I). (**J**) Size comparisons of neurites between *D. subobscura* and *D. melanogaster*. (**K**) Effects of *fru* knockdown on neurite sizes. (**L**) Effects of *fru* knockdown on NGG. (**M**) Responses of IPCs in normal (black) or Ca^{2+}-free (blue) saline upon photoactivation of the *fru* circuit or IPCs. (**N**) Comparisons of synaptic components between the two stimulation conditions. Error bars in (C) to (E), (J) to (L), and (N) represent the mean ± SD. Statistics are reported in table S6. ****$P < 0.0001$; ***$P < 0.001$; **$P < 0.01$; *$P < 0.05$; ns, not significant. Scale bars, 50 μm in (A), (H), and (I) and 10 μm in (B) and (G).

the IPC in normal saline, we succeeded in isolating synaptic inputs from the *fru* circuit to the IPC (Fig. 3, M and N). We also ran another experiment to selectively activate IPCs with *dilp2-GAL4* in the presence and absence of Ca^{2+}. In this case, no synaptic component in light-induced depolarization was detected, as expected. We conclude that functional connections exist between the *fru* circuit and IPCs in *D. subobscura*.

Overexpression of FruBM, but not FruAM or FruEM, in *D. melanogaster* IPCs induced dendrite outgrowth, phenocopying *D. subobscura* IPCs (Fig. 4, A and B, and fig. S8). To test whether extended dendrites have anatomical contact with P1 neurons, we performed double staining of the brain with two markers, IPC-specific *Dilp2-GAL4* and *R71G01-lexA*, the latter of which drives expression in the P1a subpopulation of P1 neurons (*14*, *15*). In FruBM-overexpressing IPCs, potential connections with P1 neurons were found in the superior lateral protocerebrum but not in IPCs lacking FruBM overexpression (Fig. 4C). To assess the functional relevance of the FruM-dependent dendritic remodeling, we optogenetically stimulated P1 neurons while monitoring electrical activities from a *D. melanogaster* IPC. In control IPCs without FruBM overexpression, we detected small (~4 mV) excitatory postsynaptic potentials (EPSPs) time-locked to light stimuli applied to P1 neurons (Fig. 4, D to F, and fig. S9A). We found that these EPSPs were mediated by the nicotinic acetylcholine receptor, as shown by the fact that they were blocked by d-tubocurarine (50 μM; fig. S9A).

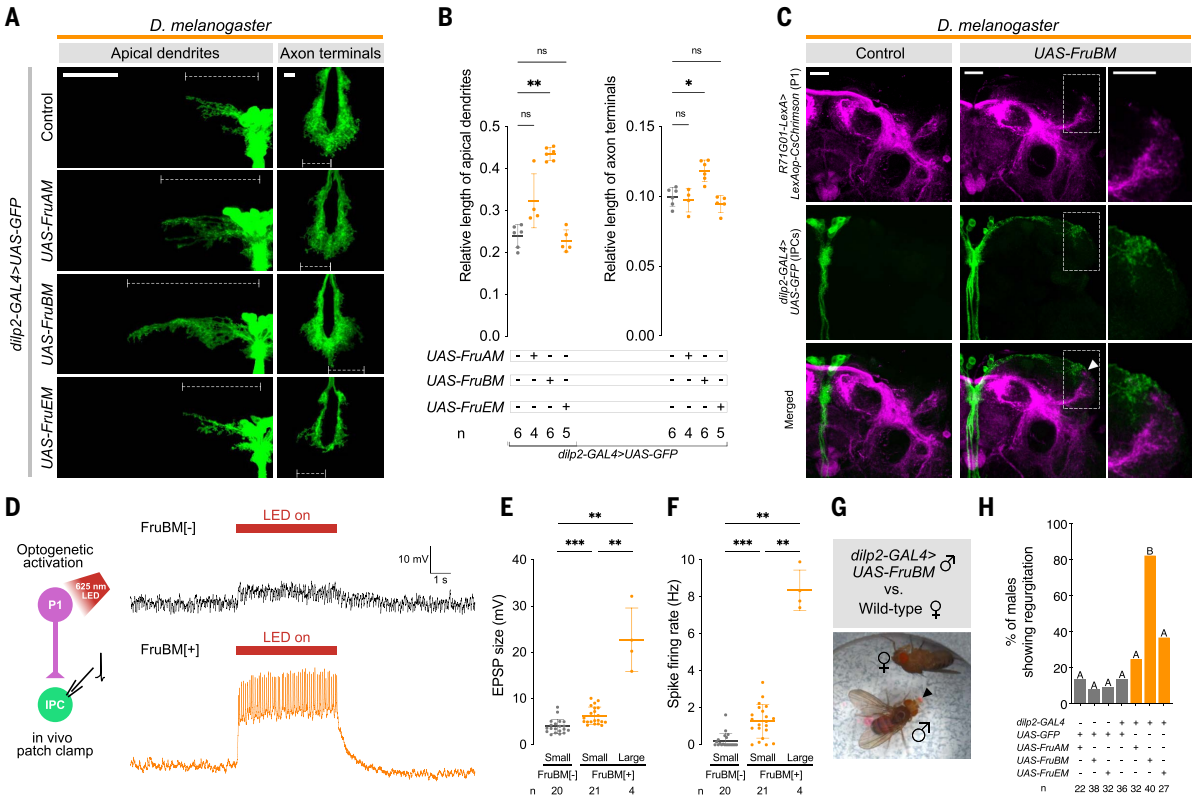

Fig. 4. Effects of FruM overexpression in IPCs on anatomy, physiology, and behavior in *D. melanogaster* males. (**A**) Dendrites (left) and terminals (right) of control or FruM-overexpressing IPCs. Scale bars, 50 μm (left) and 10 μm (right). (**B**) Effects of FruM overexpression on neurite sizes. (**C**) Stacked images of P1 neurons (top) and IPCs (middle) with (right) and without (left) FruBM and the merged images (bottom). An arrowhead indicates a possible connection site for P1 neurons and IPCs. Scale bar, 20 μm. (**D**) Voltage records from a control (FruBM[−]) and FruBM-overexpressing (FruBM[+]) IPC (right) and the experimental design (left). Horizontal bars indicate P1 stimulation (right). (**E**) EPSPs from FruBM[−] ($n = 20$) and FruBM[+] IPCs ($n = 25$). (**F**) Spike rates during P1 activation in FruBM[−] and FruBM[+] IPCs. (**G**) FruBM[+] male regurgitating during courtship. An arrowhead indicates the droplet. (**H**) Effects of FruM on regurgitation frequencies. *UAS-GFP* was used to equalize, across the genotypes tested, the copy number of *mini-w*$^+$, which has effects on fly behaviors (*28*). Bars labeled with the same letter are not significantly different ($P < 0.05$). Error bars in (B), (E), and (F) represent the mean ± SD. Statistics are reported in table S6. ***$P < 0.001$; **$P < 0.01$; *$P < 0.05$; ns, not significant.

The cholinergic input could impinge onto IPCs at the contact point with P1 neurons previously detected by GRASP (*16*). Alternatively, some unidentified cholinergic neurons might intervene between P1 neurons and IPCs to produce small EPSPs in the latter. Upon FruBM overexpression, a subset of IPCs (four of 25 cells) produced very large EPSPs of 20 mV or even larger, which initiated a train of spikes (Fig. 4, D to F, and fig. S9, A and B), whereas most IPCs with FruBM overexpression provoked only small EPSPs (Fig. 4, D and E). We did not observe similar EPSPs in IPCs without FruBM overexpression (neither the 20 IPCs in this series of experiments nor the 20 IPCs in the other experiments without FruBM overexpression). The FruBM-dependent large EPSPs were unaffected by d-tubocurarine, indicating that they represent synaptic inputs distinctly different from the cholinergic small EPSPs (fig. S9A). It remains to be determined which neurotransmitter is involved in the generation of FruBM-dependent large EPSPs. We postulate that it is the extended dendrites induced by FruBM overexpression that mediated these noncholinergic large EPSPs. Cholinergic small EPSPs were larger in IPCs with FruBM overexpression than in control IPCs (Fig. 4, E and F), and thus this synaptic potentiation also contributes to enhanced coupling between the P1-GAL4 neurons and IPCs.

Concordant with the potentiated coupling between P1 neurons and IPCs, we found that some *D. melanogaster* males overexpressing FruBM in IPCs regurgitated during attempts to lick female genitals in courtship (Fig. 4, G and H). Our close observation of courting males revealed that a few wild-type *D. melanogaster* males in fact did regurgitate during attempts to lick (Fig. 4H). Thus, FruBM overexpression in the IPCs of *D. melanogaster* males enhances regurgitation during courtship. NGG occurs between wing display and copulation attempt in *D. subobscura*, a timing analogous to that of licking in *D. melanogaster*. These observations collectively suggest that FruBM-dependent coupling of IPCs with P1 neurons is pivotal for the execution of courtship-associated regurgitation. Nonetheless, P1 neurons were not found to be a candidate for the regurgitation-inducing neurons when clonally activated in *D. subobscura* (Fig. 2C). This was partly because we could obtain only two mosaic files carrying P1 neuron clones, and neither of them showed regurgitation upon thermogenetic activation. This apparently negative result is reminiscent of the clonal activation of P1 neurons in *D. melanogaster*, in which P1 neurons successfully triggered the earlier part of courtship, including singing, yet failed to initiate the later components such as licking (*9*, *17*). Overexpression of FruAM and FruEM did not increase the occurrence of NGG (Fig. 4H), and no discernible extension of dendrites was observed. We conclude that FruBM, but not FruAM or FruEM, functions to establish the P1-IPC connections critical for the NGG induction.

Motor pathways for NGG

Some neurons in the SG were labeled more often in regurgitating than in nonregurgitating flies. These neurons were grouped as L-pSG neurons, which may include heterogeneous populations of neurons, as mentioned above. Despite this complexity, we noted that neurons with large, laterally located somata with dendrites extending to the midline

of the SG were repeatedly labeled in different mosaic males that exhibited regurgitation during thermogenetic activation (Fig. 2C). The overall structure of L-pSG neurons resembled that of some proboscis-innervating motoneurons (Fig. 2A and fig. S10A) previously reported in *D. melanogaster* (*18*–*20*). Some L-pSG neurons have an axon that exits the brain-SG complex through a peripheral nerve, indicating that they are indeed motoneurons (fig. S10A). We therefore recalculated the A-scores after dividing the L-pSG into two subclasses: L-pSG motoneurons (L-pSG-Motor) and L-pSG non-motoneurons, and compared the A-scores for L-pSG-Motor between regurgitating and non-regurgitating mosaic flies. The mosaic flies carrying *dTrpA1*-positive clones in L-pSG-Motor were substantially more enriched in the group that exhibited regurgitation upon thermogenetic activation (A-score: 33.3; four of 12 flies) than in the group that did not exhibit regurgitation (A-score: 7.6; four of 52 flies) (fig. S10B). We noted that central arborizations of the L-pSG motoneurons were juxtaposed to IPC axon terminals when three-dimensional reconstitution of these two types of neurons was registered on a template brain (fig. S10C). This finding suggests that the proboscis-innervating motoneurons may constitute a downstream pathway of IPCs.

It was difficult to deduce the cellular identity of *D. subobscura* motoneurons by analogy with their *D. melanogaster* counterparts. We therefore turned to looking for *fru*-positive motoneurons that terminate on proboscis muscles. Among the muscles we examined, muscle 9 (m9), m10, m11, and m12 [fig. S10D, terminology after (*18*)], *fru*^{so}*-GAL4*–labeled axons had terminals only on m9 in *D. subobscura* (fig. S10E). A connectome-based computational model also predicted the involvement of m9-innervating motor units in inducing proboscis extension (*21*). We therefore focused on this muscle in subsequent analyses. It remains to be rigorously tested whether these *fru*^{so}*-GAL4*–labeled axons innervating m9 indeed contain axons of L-pSG motoneurons.

Insulin neurons modulate motor outputs

The m9 muscle fibers showed spontaneous electrical activities that were characterized by repetitive volleys of depolarizing potentials: a single volley of 1.36 ± 0.15 s (mean ± SD) in duration and 11.00 ± 7.17 mV (mean ± SD) in amplitude occurred with intervals of 6.67 ± 1.81 s (mean ± SD; n = 13; Fig. 5, A to C). A volley consisted of several types of EPSPs, each different in size, which collectively formed a large, depolarizing plateau (Fig. 5, B and C). Unilateral severing of the pharyngeal nerve eliminated phasic EPSP volleys and compromised contraction of the proboscis muscle m9 on the operated side while sparing these EPSPs and muscle contraction on the nerve-intact side (compare Fig. 5B for EPSPs). This observation

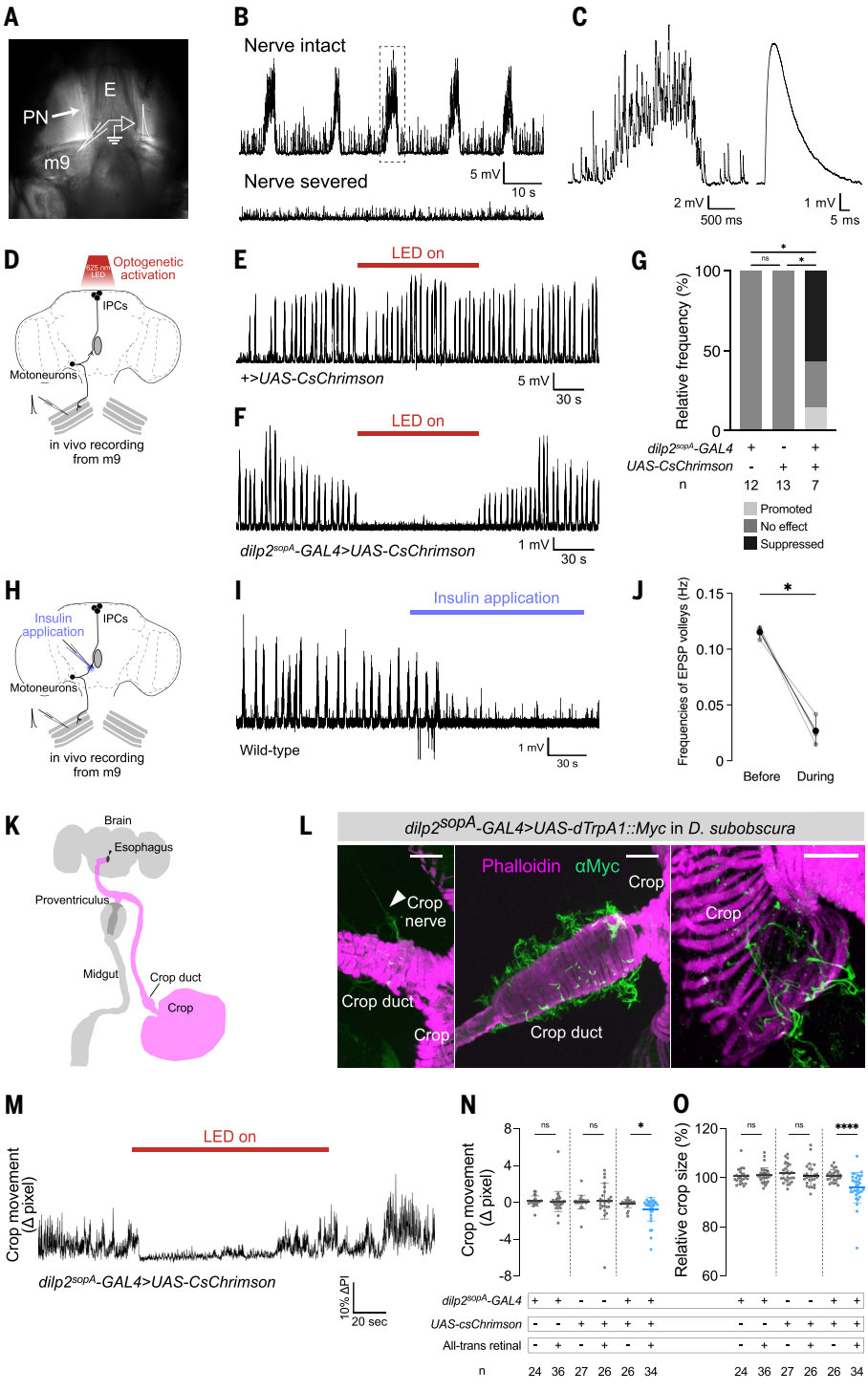

Fig. 5. IPCs suppress motor outputs in *D. subobscura* males. (**A**) Preparation for m9 electrophysiology. PN, pharyngeal nerve. E, esophagus. (**B**) Spontaneous activities in m9 when the PN is intact (top) or severed (bottom). (**C**) The boxed portion in (B) shown with two expanded time scales. (**D**) The recording system. (**E** to **G**) Effect of IPC activation (horizontal bars) on m9 activities in control (E) and test (F) flies and quantification of the effect (G). The proportions of flies in which EPSP volleys in m9 were promoted (pale gray), suppressed (black), or unaffected (gray) upon IPC activation is shown. (**H**) Schematic of an iontophoresis experiment. (**I** and **J**) Example (I) and quantification (J) of responses to insulin iontophoresis. (**K**) Schematic of the brain and digestive organs. (**L**) IPCs innervating the crop through the crop nerve (arrowhead). Scale bar, 50 μm. (**M**) Example of movement records showing the effect of IPC activation (horizontal bar). (**N**) Quantification of the crop movement (mean ± SD). (**O**) Quantification of the crop size. Error bars in (J), (N), and (O) represent the mean ± SD. Statistics are reported in table S6. ****P < 0.0001; **P < 0.01; *P < 0.05.

implies that m9 is controlled by the *fru*-positive motoneuron that innervates this muscle through the pharyngeal nerve. These electrical activities in m9 seem to be associated with spontaneously occurring partial extension of the proboscis: The average rate of volleys (0.161 ± 0.047 Hz, $n = 13$) was close to that of partial extension events (0.160 ± 0.124 Hz, $n = 4$). In most cases, optogenetic activation of IPCs immediately suppressed the occurrence of these EPSP volleys in m9 (Fig. 5, D to G). Likewise, iontophoretic application of insulin onto the SG neuropilar region where IPCs terminate almost immediately suppressed the generation of EPSP volleys (Fig. 5, H to J). The short latency of responses to a focally applied ligand suggests that insulin directly acted on the input synapses of motoneurons. Insulin has been shown to exert an acute inhibitory effect on excitatory transmission by reducing presynaptic release in the mouse hippocampus (*22*). McKeller *et al*. (*18*) showed in *D. melanogaster* that m9 acts as a protractor of the rostrum and at the same time as an extensor of the haustellum, leading to the downward extension of the proboscis upon activation of the innervating motoneuron mn9. The same authors also reported that the haustellum is flexed, rather than extended, when males perform licking, during which time the proboscis is extended anteriorly (*18*). In fact, they found that silencing mn9 inhibited the extension of the haustellum (*18*), which was thus kept flexed as in the case of courtship licking. We confirmed in *D. subobscura* that males extend their proboscis anteriorly for NGG and downwardly for feeding (movies S1 and S3). When IPCs were optogenetically activated during feeding, downward extension was interrupted by repetitive upward (and anteriorly directed) movements of the proboscis, resulting in spasms (fig. S11A and movie S4). By contrast, suppression of IPCs during courtship reduced the frequency of anterior proboscis extension (fig. S11B). Taking these results together, we postulate that IPCs modulate motor outputs to m9 within the central circuit that controls NGG. Close inspection of IPC morphology in *D. subobscura* revealed a prominent lateral extension of axon terminals, which overlapped with dendritic arbors of the L-pSG motoneurons, when two images of clonally labeled neurons were overlaid on a template brain (fig. S10C). The formation of extended terminals was abrogated by *fru* knockdown in *D. subobscura* IPCs (Fig. 3, I and K). In contrast to *D. subobscura* IPCs, *D. melanogaster* IPCs have no discernible lateral extension of terminals. We posit that the extended terminals could mediate the suppressive effect of IPC activation on motor output to m9 in *D. subobscura*.

IPC activity induces crop constriction

As in *D. melanogaster*, IPC axons form terminals on the crop in addition to the SG in *D. subobscura* (Fig. 5, K and L) (*23*). We found that optogenetic stimulation of IPCs with CsChrimson reduced crop movements in *D. subobscura* (Fig. 5, M and N). It is inferred that a reduced movement permits digested food to stay in the crop, and then this food can be allocated to produce a droplet as a nuptial gift. Furthermore, we found that IPC activation decreased the crop size in *D. subobscura* (Fig. 5O). This decrease in crop size could help to elicit regurgitation for NGG by increasing the internal pressure of the crop.

Discussion

IPCs appear to coordinate two important effectors operating for NGG, the proboscis and crop, through two distinct motor pathways. Our analysis favors a model in which IPCs are activated by P1 neurons, which strongly drives execution of species-specific male courtship behavior in *D. subobscura* (fig. S12). IPCs of *D. subobscura*, but not *D. melanogaster*, males express the male-specific *fru* product FruM. A tantalizing possibility is that the expression of specific adhesion molecules in *fru* neurons might promote their interconnection to establish the functional *fru* circuit for executing courtship behavior. Two established transcriptional targets of FruM, *robo1* (*24*) and *tei* (*25*), belong to the gene superfamily encoding immunoglobulin-like domain adhesion proteins, and many of the immunoglobulin superfamily members participate in neurite targeting (*26*, *27*). In fact, we found *D. subobscura*–specific extensions of IPC neurites that formed in *D. subobscura* in a FruM-dependent manner. These FruM-dependent extended neurites appeared to mediate connections of IPCs with courtship initiator P1 neurons and proboscis-innervating motoneurons, both of which express FruM. We presume that this expansion of FruM expression domains was a prerequisite for the recruitment of IPCs to the courtship circuit, which conferred on *D. subobscura* males the latent ability to perform NGG, in which regurgitation plays a central role.

REFERENCES AND NOTES

1. E. Immonen, A. Hoikkala, A. J. N. Kazem, M. G. Ritchie, *Behav. Ecol.* **20**, 289–295 (2009).
2. R. H. Steele, *Anim. Behav.* **34**, 1087–1098 (1986).
3. R. Tanaka, T. Higuchi, S. Kohatsu, K. Sato, D. Yamamoto, *J. Neurosci.* **37**, 11662–11674 (2017).
4. H. T. Spieth, *Bull. Am. Mus. Nat. Hist.* **99**, 395–474 (1952).
5. M. V. Hernández, C. C. Fabre, *J. Insect Behav.* **29**, 578–590 (2016).
6. H. Ito *et al.*, *Proc. Natl. Acad. Sci. U.S.A.* **93**, 9687–9692 (1996).
7. L. C. Ryner *et al.*, *Cell* **87**, 1079–1089 (1996).
8. S. Cachero, A. D. Ostrovsky, J. Y. Yu, B. J. Dickson, G. S. X. E. Jefferis, *Curr. Biol.* **20**, 1589–1601 (2010).
9. K. Kimura, T. Hachiya, M. Koganezawa, T. Tazawa, D. Yamamoto, *Neuron* **59**, 759–769 (2008).
10. J. Y. Yu, M. I. Kanai, E. Demir, G. S. X. E. Jefferis, B. J. Dickson, *Curr. Biol.* **20**, 1602–1614 (2010).
11. J. G. Stoffolano Jr., A. T. Haselton, *Annu. Rev. Entomol.* **58**, 205–225 (2013).
12. Y. D. Chen, S. Ahmad, K. Amin, A. Dahanukar, *J. Exp. Biol.* **222**, jeb210724 (2019).
13. D. R. Nässel, O. I. Kubrak, Y. Liu, J. Luo, O. V. Lushchak, *Front. Physiol.* **4**, 252 (2013).
14. L. F. Seeholzer, M. Seppo, D. L. Stern, V. Ruta, *Nature* **559**, 564–569 (2018).
15. F. A. Roemschied *et al.*, *Nature* **622**, 794–801 (2023).
16. L. Zhang, X. Guo, W. Zhang, *Sci. Adv.* **8**, eabl6121 (2022).
17. S. Kohatsu, D. Yamamoto, *Nat. Commun.* **6**, 6457 (2015).
18. C. E. McKellar, I. Siwanowicz, B. J. Dickson, J. H. Simpson, *eLife* **9**, e54978 (2020).
19. A. Manzo, M. Silies, D. M. Gohl, K. Scott, *Proc. Natl. Acad. Sci. U.S.A.* **109**, 6307–6312 (2012).
20. O. Schwarz *et al.*, *eLife* **6**, e19892 (2017).
21. P. K. Shiu *et al.*, *Nature* **634**, 210–219 (2024).
22. F. Zhao, J. J. Siu, W. Huang, C. Askwith, L. Cao, *Neuroscience* **411**, 237–254 (2019).
23. Y. Ohhara, S. Kobayashi, K. Yamakawa-Kobayashi, N. Yamanaka, *J. Comp. Neurol.* **526**, 1351–1367 (2018).
24. H. Ito, K. Sato, S. Kondo, R. Ueda, D. Yamamoto, *Curr. Biol.* **26**, 1532–1542 (2016).
25. K. Sato, H. Ito, D. Yamamoto, *Commun. Biol.* **3**, 598 (2020).
26. J. R. Sanes, S. L. Zipursky, *Cell* **181**, 536–556 (2020).
27. Q. Xie *et al.*, *Neuron* **110**, 2299–2314.e8 (2022).
28. S. D. Zhang, W. F. Odenwald, *Proc. Natl. Acad. Sci. U.S.A.* **92**, 5525–5529 (1995).

ACKNOWLEDGMENTS

We thank the Bloomington *Drosophila* Stock Center for fly stocks; M. Adachi for secretarial assistance; R. Nishimura at the Technical Center of Nagoya University for constructing the chambers used in the behavioral experiments; H. Toda for critical discussion; and Y.-J. Kim for a DNA plasmid. **Funding:** This work was supported by Grants-in-Aid for Scientific Research from the Ministry of Education, Culture, Sports, Science and Technology (grant 21H04790 to D.Y. and grants 19K16186, 21K15137, 22H05650, 23K05846, and 24H01433 to R.T.). **Author contributions:** Access to tools and facilities: T.A., A.K.; Conceptualization: R.T., D.Y.; Data analysis or interpretation; R.T., Y.H., S. Kohatsu, K.S., H.M., T.H., T.A., A.K., D.Y.; Funding acquisition: R.T., D.Y.; Genome sequence analysis and creation of the genome database: S. Kondo, A.T.; Investigation: R.T., Y.H., H.M., T.H.; Methodology: R.T., Y.H.; Project administration: R.T., D.Y.; Supervision: R.T., D.Y.; Visualization: R.T., Y.H.; Writing – original draft: D.Y.; Writing – review & editing: R.T., D.Y., Y.H. **Competing interests:** The authors declare no competing interests. **Data and materials availability:** All data are available in the main manuscript or the supplementary materials. The nucleotide sequence data reported are available in the DDBJ/EMBL/GenBank databases under accession numbers LC868266 and LC868267. All constructs, antibody, and transgenic fly strains developed in this study are available upon request.

SUPPLEMENTARY MATERIALS

science.org/doi/10.1126/science.adp5831
Materials and Methods; Figs. S1 to S15; Tables S1 to S6; References (*29*–*42*); MDAR Reproducibility Checklist; Movies S1 to S4; Data S1 and S2

Submitted 2 April 2024; accepted 14 May 2025

10.1126/science.adp5831